Article

Experimental Performances Evaluation on Counter-Rotating Coaxial Propellers for Multirotors

Nicola Russo , Aniello Daniele Marano , Giuseppe Maurizio Gagliardi [*] , Michele Guida , Tiziano Polito , Francesco Marulo

Article

Thrust and Noise Experimental Assessment on Counter-Rotating Coaxial Rotors

Nicola Russo [1], **Aniello Daniele Marano** [1,†] , **Giuseppe Maurizio Gagliardi** [1,*] , **Michele Guida** [1] , **Tiziano Polito** [1] and **Francesco Marulo** [1]

[1] Industrial Engineering Department, University of Naples Federico II, via Claudio 21, Napoli.
* Correspondence: giuseppemaurizio.gagliardi@unina.it
† Current address: AVIO - Advanced Vision Into Orbit, Colleferro RM.

Abstract: Multirotors are gaining great importance in the layout of innovative and more agile mobility. In this framework, a possible solution to developing an aircraft complying with the stringent size requirements characterizing this type of application can be a coaxial rotor configuration. To exploit the several possibilities linked to coaxial rotors, a scaled experimental model is designed to evaluate the performances of the counter-rotating propellers system, concerning the distance between the two propellers. Both thrust and noise are considered as parameters of interest. Two brushless motors are deployed whereas the propellers' angular velocity, in terms of round per minute (rpm), is controlled by an external control system. Tests are conducted on both single isolated propellers as well as on the counter-rotating system: the two propellers and their respective motors have been characterized concerning the thrust. Furthermore, a comparison with a numerical model is performed. Noise evaluation on the single propeller has shown a motor contribution prevalence at a low rpm regime (1140-1500 rpm) and a propeller prevalence for angular velocities higher than 1860 rpm. By varying the distances between the propellers a sensitivity analysis is performed with the aim of identifying the optimum configuration taking into account both noise and thrust performances.

Keywords: multirotors; coaxial rotors; counter-rotating propellers; thrust performances; noise

---

1. Introduction

In the last few years, for a fast and reliable point-to-point connection or intercity flights and to solve the runway congestion problem, the Runway-Independent Aircraft concept is increasingly becoming more prominent in civil aviation. Moreover, the market prospects predict an increasing demand for Disc-Rotor technologies in the Civil field: business flights, air medical, search and rescue applications, and others.

Multirotors are gaining great importance in the layout of innovative mobility: until now, Unmanned aerial vehicles (UAVs) and, more in general, electric aerial vehicles have mostly been used for surveillance, system maintenance, monitoring, and recreative purposes. The possibility of extending multirotor technologies to human and cargo transportation in the urban environment has led to a revolution in the way we intend the third dimension. This layout will presumably represent a new disruptive airborne technology [1]. The Vertical Flight Society (VFS), the world's leading non-profit organization working to advance vertical flight, has recently announced [2] that the number of electric vertical takeoff and landing (eVTOL) aircraft concepts being tracked in its World eVTOL Aircraft Directory has reached 600 designs from nearly 350 companies worldwide. In this framework, several companies are developing electrical vertical take-off aircraft (eVTOL) which are equipped with different propeller configurations.

A multirotor is a rotorcraft with more than two lift-generating rotors. Unlike single helicopters which use complex variable pitch rotors whose pitch varies as the blade rotates for flight stability and control, multirotors often use fixed-pitch blades. Control of vehicle motion is achieved by varying the relative speed of each rotor to change the thrust and torque produced by each [3–6].

Due to its inherently good performances, the coaxial propellers configuration has been used for many

years for fixed wings aircraft [7]. The coaxial propellers main goal should be to increase efficiency which leads to a power-saving triggered by the possibility of decreasing the rotational induction associated with the motion of the propeller [8–12]. This technology has been widely implemented and adapted for rotor-based aircraft such as helicopters and, lately, drones and, in general, UAVs [13,14]. The employment of Counter-rotating propellers has been recently evaluated for an Octocopter Drone application in [15]. Also, the possibility to use partial overlapping propellers has been studied [16]. In general, the problem of the coaxial or (partial) overlapping propellers is their noise. In last years, the prediction of propellers acoustics has become increasingly important because of the more and more stringent aircraft noise requirements. However, aeroacoustic simulations have historically relatively simple flow field models and approximations. Because of that, several works have been developed in the latest period both to predict propellers' noise [17–19] and enhance their design [20]. A common issue of these methods is their validation. A few experimental data are available in the literature for these applications. This work is also intended to provide an experimental database for future methods development and validation.

Over the past few years, several unmanned aerial vehicles have been oriented to an increasing spectrum of end-users thanks to the possibility of having smaller, lighter, and quieter systems capable of operating in highly congested areas without compromising on both the hovering and the take-off and landing capabilities.

The main scope of this work consists of the analysis of both thrust and noise performances of a scaled model of counter-rotating coaxial propellers as the distance between the propellers varies. The two propellers performance parameters taken into account are the *Thrust* (measured in kg) and the *Noise level* (measured as A-weight equivalent continuous sound level $L_{A_{eq}}$). The thrust is able to define the lifting capability of the configuration while the $L_{A_{eq}}$ has been selected to estimate the environmental impact of the configuration [21–24].

The tests were carried out on two different configurations: both the propellers were tested in isolated conditions to provide a reference and in coaxial counter-rotating flow to perform the test of actual interest. The experimentally obtained thrust has been also compared with numerical results with satisfactory agreement.

2. The experimental setup: from concept to implementation

A dedicated test facility has been designed based on the possibility of both changing the distance between the two propellers as well as evaluating their optimum position with respect to the ground. The structure has been designed to place all the necessary electronics for both the load cell acquisition system, the angular velocity controller and power supply for the two independent lines. An overview of the experimental set-up is shown in Figure 1.

In more detail, the testing facility has been designed by adapting a metallic shelving with cantilever supports stabilized by the weight of the horizontal shelves. Employing some angular support, a vertical component, perpendicular to the ground, allows the propeller axial motion and centering. The position of the cantilever rack can be modified by selecting one of the multiple positions available on the structural external components: by applying this logic it is possible to tune the distance between the propeller in both a coarse and precise way by varying, respectively, the position of the cantilever component, and the position of the axial arm. The support structure consists of a cantilever rack, composed by 4 single side columns, 4 800 mm arms and accessories like caps and pins. Two vertical rods are intended to support the engines, the load cells and the propellers. In particular, a couple of aluminum L-shaped rods 60x60 mm with a groove of 10, type B, 1300 mm long, and a couple of aluminum L-shaped rods 60x60 mm with a groove of 10, type B, 750 mm long are used.

It is important to notice that the blue arms are allowed to slide vertically to reach an appropriate distance from the ground and a proper spacing between the two propellers. By changing the position of the cantilever arms, a coarse trim can be performed. The correct placing of the arm is guaranteed by means of a rigid pin secured with a split pin. The overall structure, able to provide a coarse position

trimming of the propellers, is shown in Figure 2. For a more accurate separation, two horizontals supports have been positioned on the cantilever arms and secured to the horizontal supports with two angular connecting staffs. The Figure 2 shows the rig in its final theoretical configuration.
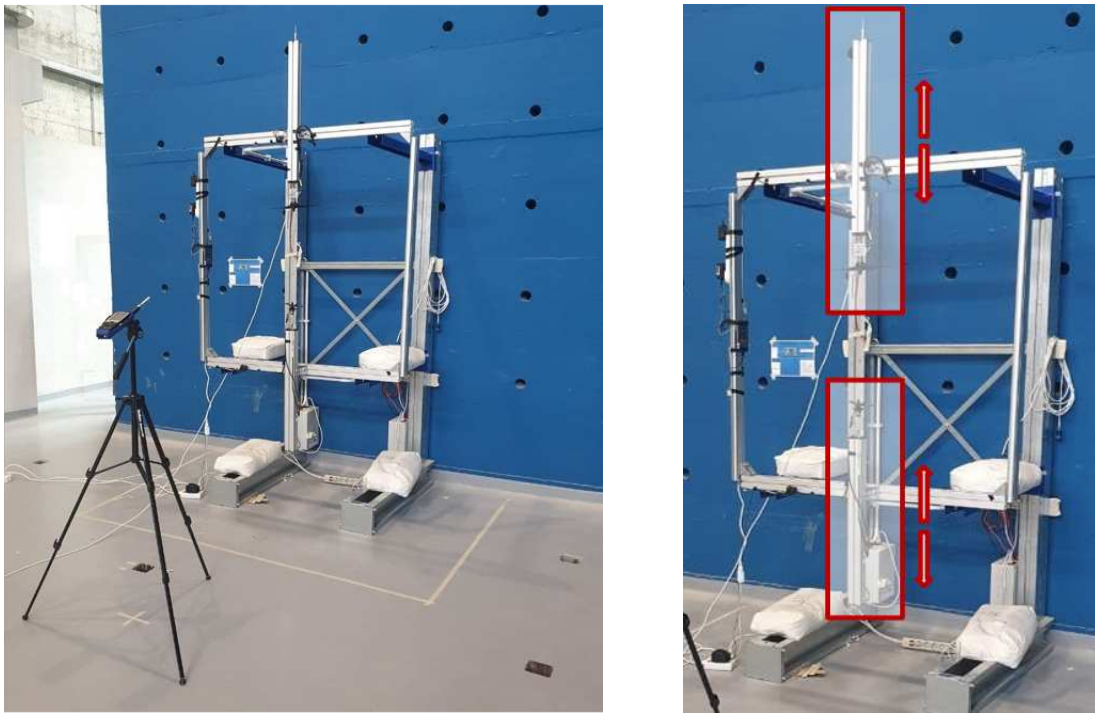

**Figure 1.** An overview of the experimental set-up.

Figure 2. Rig final theoretical configuration: CAD model (left) and construction (right).

Another set of two additional components has been added to secure axial centering of the propellers. The most critical component of the system is represented by the vertical movable arm that has been realized by integrating the grooved component with a 50 kg traction and compression load cell and a metallic interface directly connected with the electric motor. The load cells have been centered by means of a 3D printed component in which a M6 threaded rod has lately been adjusted.

The over mentioned configuration provides a good centering of the threaded rod which is lately screwed into the M6 load cell threaded hole. The metallic component shown on the right side of the Figure 3 is the electric motor support whose threaded stem is designed to be coupled directly with the load cell. Also, the overall vertical arm assembly is shown. A brushless motor rigidly mounted on the T-motor support completes the test facility shown in Figure 4.
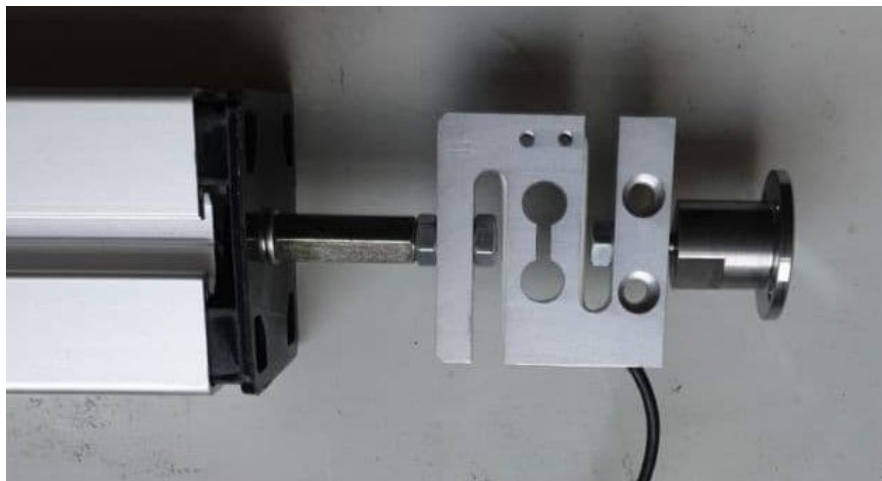
Figure 3. Vertical arm assembly, from the left: arm-load cell interface, load cell, T-motor support.
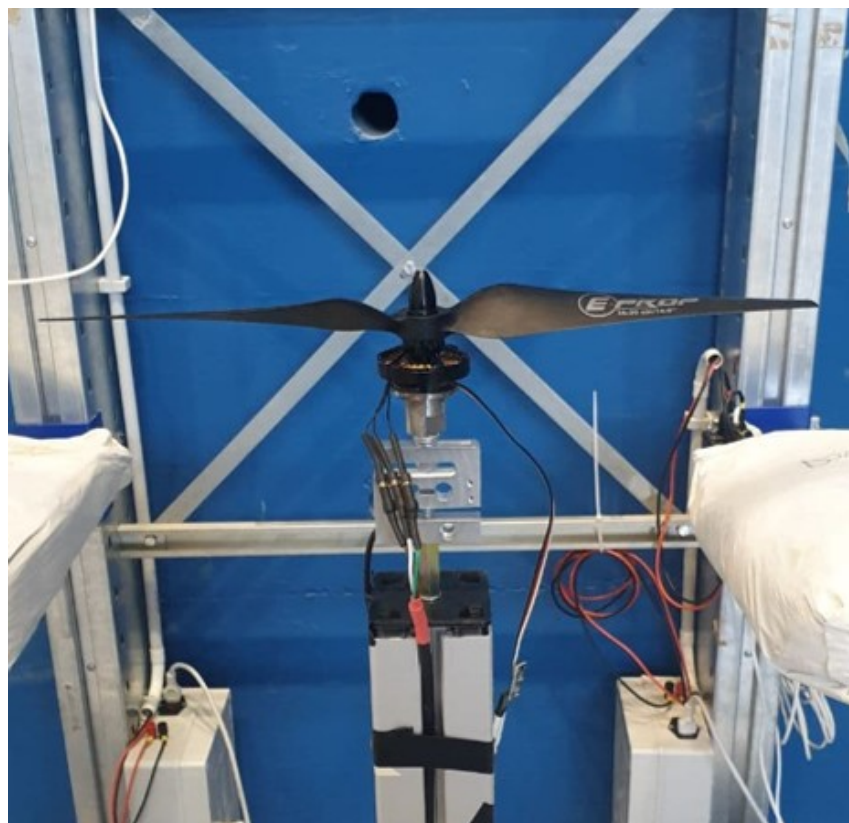
Figure 4. Complete vertical arm configuration.

The whole system does, therefore, consist of all the mechanical components listed previously and a brushless motor that is mounted rigidly on the T-motor support. An essential part of the experimental setup is represented by the electronic system. It is important to notice that several different sub-systems are integrated to control the propellers, allow the propeller's angular speed modification, measure the thrust generated by the propellers, evaluate the noise produced by the whole system. To better characterize the electronics, every single component is described separately with its software and hardware implications.

2.1. The propeller angular velocity control system

One of the main purposes concerning experimental testing is the evaluation of the thrust of the propellers as a function of the angular velocity of the propellers themselves. To perform this task, an rpm control system has been developed to provide a good level of control for the two independent lines. The main scope of the control system is the supply of the T-motors, the regulation of their angular velocity concerning the target value provided with the handheld controller, and the visualization of both the target value and the reached one.

The control system implements a *"closed ring"* logic to the rotational speed of the two propellers: two independent generators of a Pulse Wave Modulation (*PWM*) signal that is later fed to the two Electronic Speed Controllers (*ESC*). The ESC regulates the power supply to the motors and, as a consequence, the angular velocity of the motor itself. The actual value of the angular velocity is measured with a magnet HALL sensor; the difference between the commanded rpm value and the actual value is then elaborated by a correction controller that imposes an acceleration/deceleration up to the stabilization of the angular velocity. The Figure 5 shows the sensor and control system.
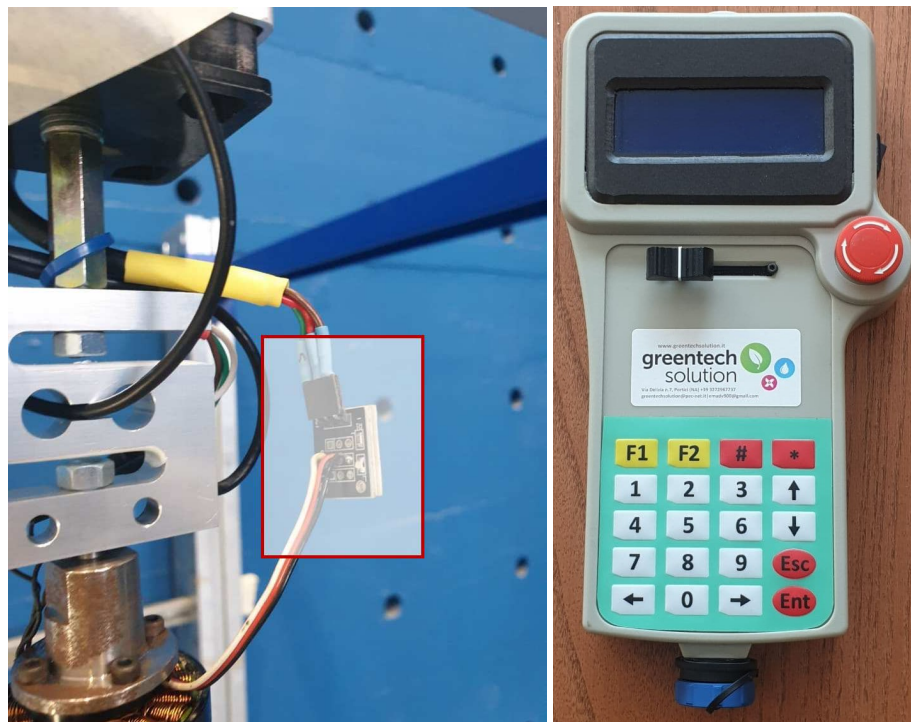

Figure 5. Magnetic Hall effect sensor (left) and handheld computer (right).

Two 400 kV Specs brushless T-motor have been deployed to provide propeller's motion. This kind of motor is particularly indicated for drone application since it provides good thrusts without compromising on its weight (53 g). This motor, specific for 15-18" propellers, it has an internal resistance of 452 mΩ and a maximum continuous power of 216 W [25].

6 of 17

2.2. The load cell acquisition system

The load cell acquisition system has been designed to operate with *National Instruments* (NI) products: LabVIEW software and NI myRIO-1900 have been deployed as, respectively, programming environment and hardware. The myRio board was connected with the load cell which provides an analog signal within a range of mV.

The 50 kg bidirectional load cell consists of an aluminum *s-shaped* load cell; it is designed to work with both traction and compression loads. The supply tension is in a range of $9 - 12\,V$ and its nominal sensitivity is $2.0 \pm 0.1\,mV/V$. The cell is reported to be particularly indicated for suspended loads. Due to the operating range, a signal digitizer was necessary: the HX711 board, supplied with an external source was used [26]. This precision 24-bit analog to digital converter, designed for weighing scales and widely used in industrial applications, features two differential input channels and an active low noise PGA with a selectable gain of 32, 64, 128. Since the operating supply voltage range is $2.6 - 5.5\,V$, it can be easily fed with the myRio-1900 output port. This component interfaced directly with the myRio-1900 and provides both data and clock measurement [27].

The load cell acquisition system has been also developed in its software part. The programming environment choice has been LabVIEW. The interface with the digitizer has been originally intended for Arduino applications, and the myRio and a control panel for easy management of the acquisition has been projected.

3. Test Results

The performances of the two propellers have been experimentally evaluated in the case of isolated and coupled functioning. Also, their noise characterization has been performed. The investigation has been conducted at different angular speeds. The current chapter summarises the results of the thrust and noise characteristics for both the isolated and coupled conditions.

3.1. Isolated propeller and T-motor characterization

Before proceeding with the two propeller systems, an isolated propeller thrust characterization has been performed by considering just one active propeller at a time; the obtained results have been also used to implement an XROTOR numerical model.

The noise characterization has been conducted in two different experimental conditions: T-motor and T-motor + propeller run at the same angular velocity. Both tests have been conducted by measuring the thrust generated by the propeller over a 30 s period starting from the reach of the steady state. Let us notice that from a controller's logic point of view, the steady state condition was reached when the actual velocity of the propeller corresponded with the target velocity ±60 rpm. This condition was named the governor *lock-ok* condition.

3.1.1. Single propeller thrust evaluation

The diameter of the propeller is $D = 36\,cm$. The test facility has been arranged to place the propellers at a 1.5D distance from each other and a 1D distance from the supporting horizontal arm. The test setup for the isolated propeller condition is shown in Figure 6. The isolated propeller hypothesis has been fulfilled by considering only one active propeller at the time.

A simple procedure for the acquisition has been set to ensure the appropriate repeatability of the testing campaign. Each acquisition has been carried out for 30 s from the *lock-ok* condition (steady state). To highlight the experimental characteristics of the data set and to provide a comparison with XROTOR numerical results, an error bar diagram has been chosen.
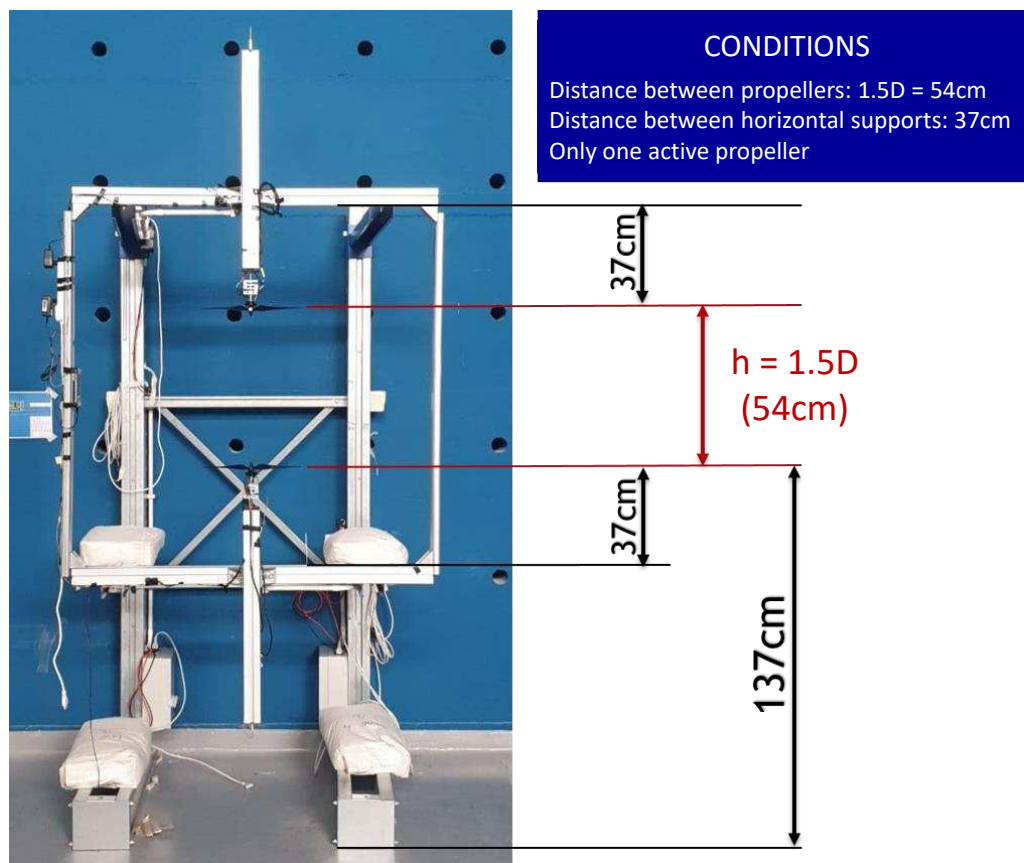
Figure 6. Experimental setup for the isolated propeller condition.

Several information can be derived from the chart in Figure 7: at low rpm, the isolated lower propellers curve and the isolated upper propellers curve exhibit lightly different performances in terms of mean thrust value. This behaviour could have been attributable to some aerodynamic reasons. The two propellers are supposed to be identical from an aerodynamic and geometric point of view. The difference lies in the opposed arrangement of the two propellers. In the upper propeller case, the support is located at the top of the propeller and its wake is free from obstacles. In the lower propeller case, the pillar is located at the bottom of the disk resulting in a disturbance of the wake region. An ulterior motivation is due to the partial ground effect on the upper propeller caused by the lower one. The distance between the two propellers is enough small to generate the ground effect [28–31]. For some angular velocities, the lower propeller also rotated due to the swirl effect caused by the wake of the upper one [32]. This caused a parachute effect similar to the one characterizing the helicopters during the autorotation phase [33–35]. In this condition, the generated ground effect is even larger.

It could also be highlighted that no measurement was possible in a range between [1020-1500] rpm for both the propellers due to a first resonance of the supporting vertical arm; another more serious resonance has been detected in a [1900-2820] rpm range for the upper propeller. This issue is caused by a transversal motion of the centering frame that is triggered by the compression load generated due to the upper propeller motion. In correspondence with this resonance, a rotational motion of the threaded connecting bar leads to a torque applied on the load cell. The load cell's motion determines a modification of the electronic configuration of the load cell-digitizer interface which results in a zero reference loss. To avoid such an issue, it has been decided to perform the testing up to 1900 rpm, disconnect the system, check for possible non-compliance in the zero-reference value and restart the test. The second resonance range has been avoided accelerating the system straight from 0 up to a 2820 rpm angular velocity: this method has shown good results since, a quality control

performed on the zero value and the reference value once the testing has been interrupted, has proven accordance between the pre and post resonance thrust values.
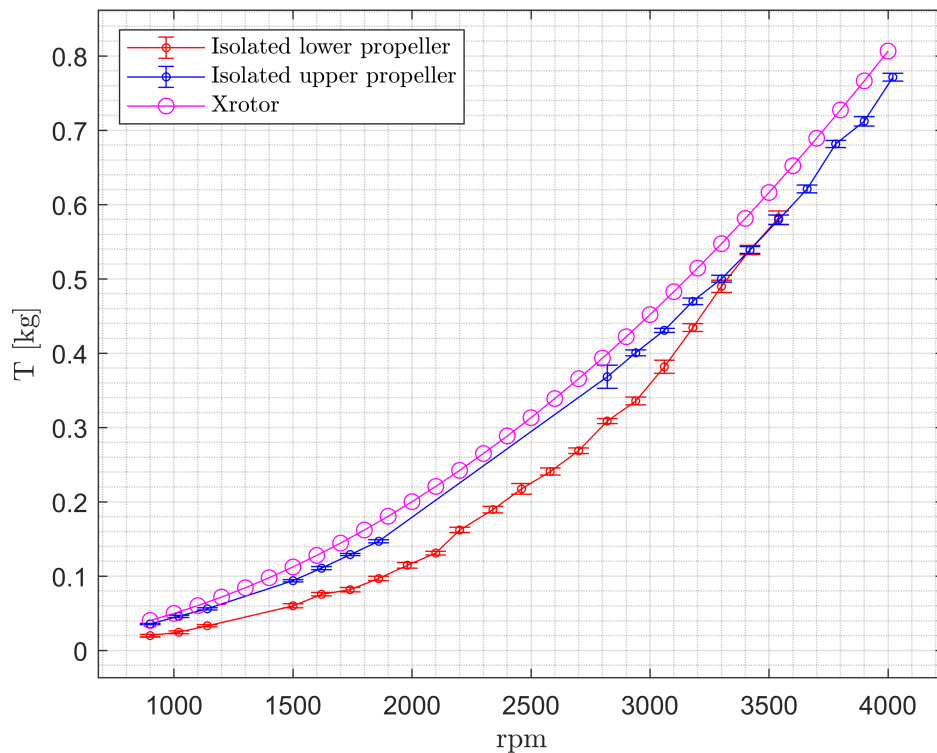
Figure 7. Thrust variation varying rpm for the isolated propellers.

3.1.2. Single propeller noise characterization

The system has been characterized from an acoustic point of view to understand the contribution of both the propeller and the T-motor and to highlight the frequency content for different values of the angular velocity. The $L_{A_{eq}}$ parameter, which has been measured by means of an NTi Audio XL2 sound level meter [?], is shown in Figures 8-11. Two configurations have been tested: T-motor (motor running without the propeller) and T-motor + propeller. The microphone was positioned 1.5m away from the propeller's hub into their rotation plane, perpendicular to the ground. The sampling frequency was set at 51 kHz while the timestep (integration time) of the equivalent level was set at 100 ms.
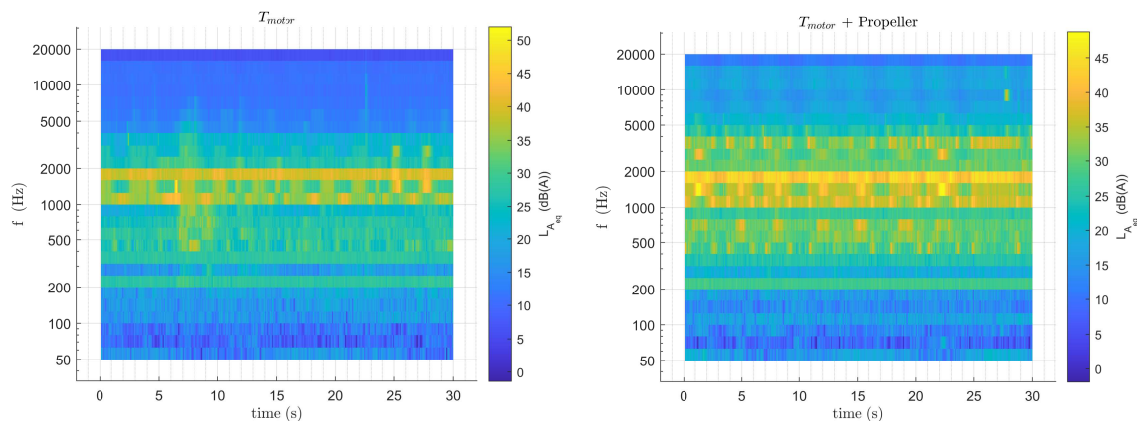
Figure 8. $L_{A_{eq}}$ spectrogram at 900 rpm - Tmotor(left), Tmotor + propeller (right).
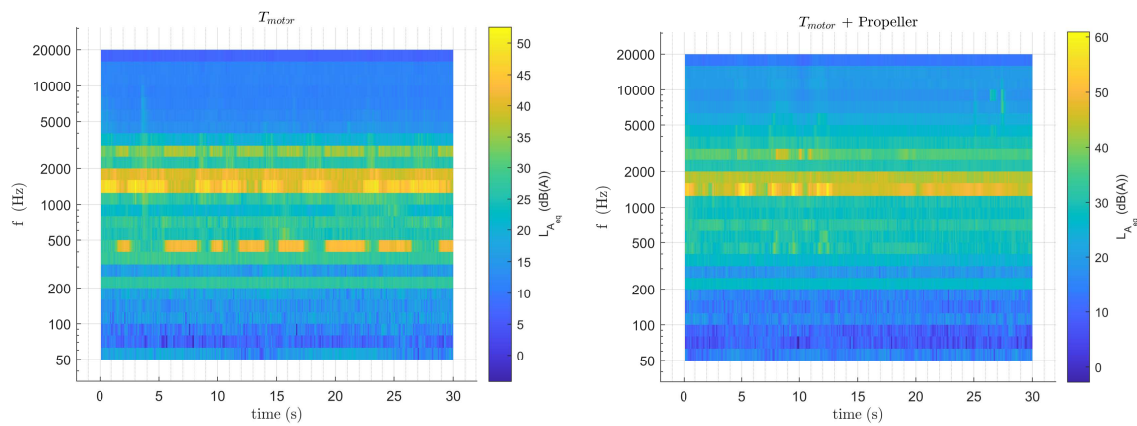
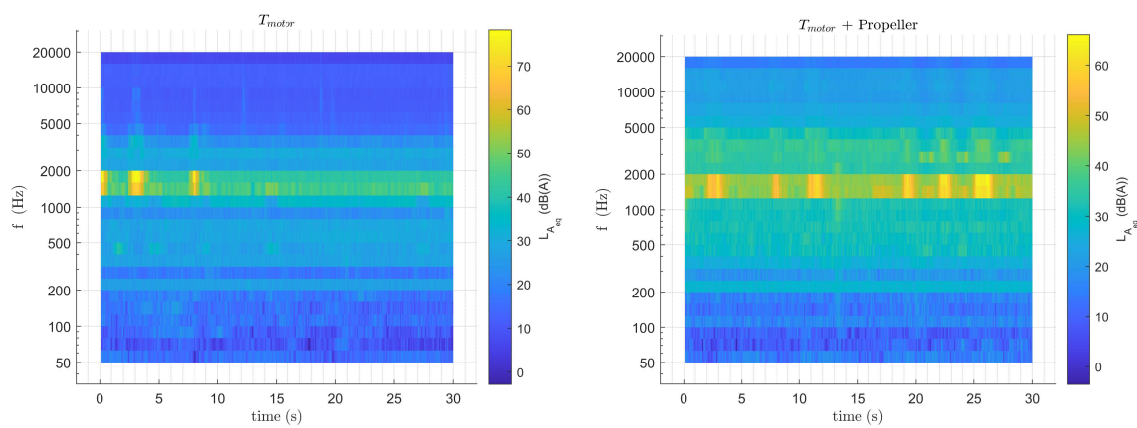**Figure 9.** $L_{A_{eq}}$ spectrogram at 1020 rpm - Tmotor(left), Tmotor + propeller (right).

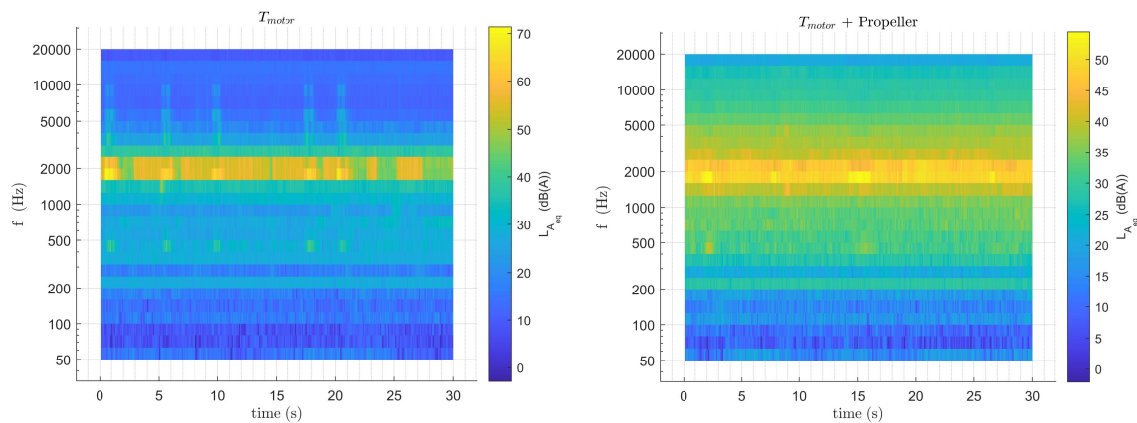**Figure 10.** $L_{A_{eq}}$ spectrogram at 1140 rpm - Tmotor(left), Tmotor + propeller (right).

Figure 11. $L_{A_{eq}}$ spectrogram at 1500 rpm - Tmotor(left), Tmotor + propeller (right).

By observing the charts of the $L_{A_{eq}}$ vs time for both propeller and T-motor + propeller configurations, it is possible to notice that the $L_{A_{eq}}$ measured in by the T-motor + propeller configuration is not always prevalent on the $L_{A_{eq}}$ generated by the T-motor itself. From Figure 9, high peak oscillations are highlightable: this results in distinct tones. It is also possible to emphasize that, at a lower rpm regime, higher periodic oscillation occurs: those are determined by the angular velocity control system which has been reported to be activated with higher frequency.
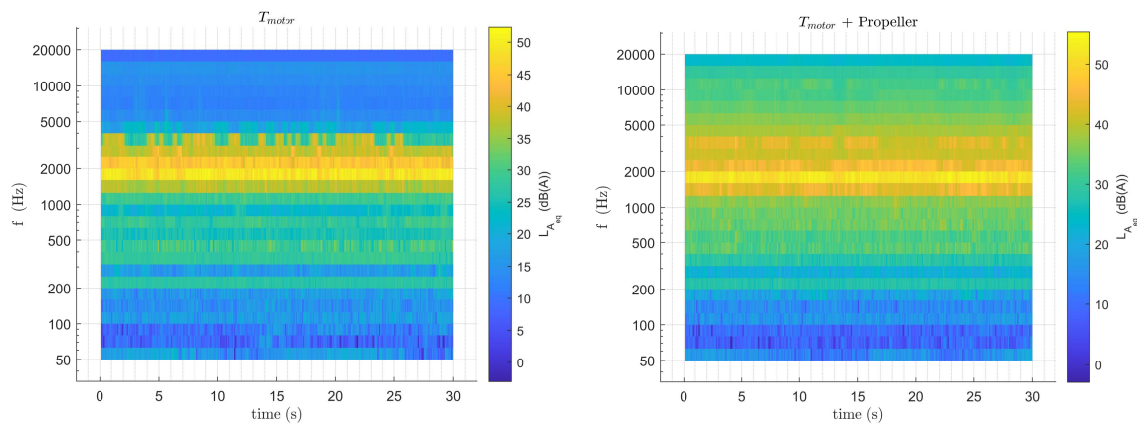
Figure 12. $L_{A_{eq}}$ spectrogram at 1620 rpm - Tmotor(left), Tmotor + propeller (right).
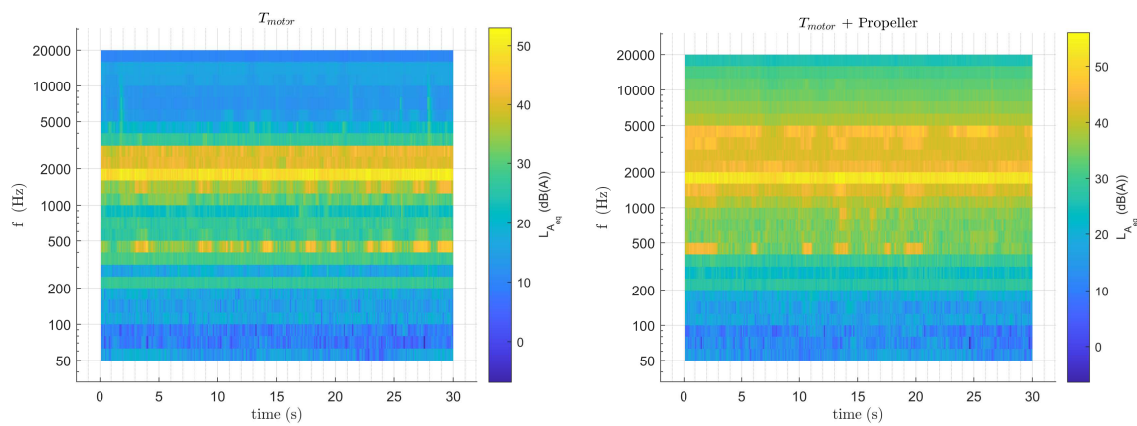

Figure 13. $L_{A_{eq}}$ spectrogram at 1740 rpm - Tmotor(left), Tmotor + propeller (right).
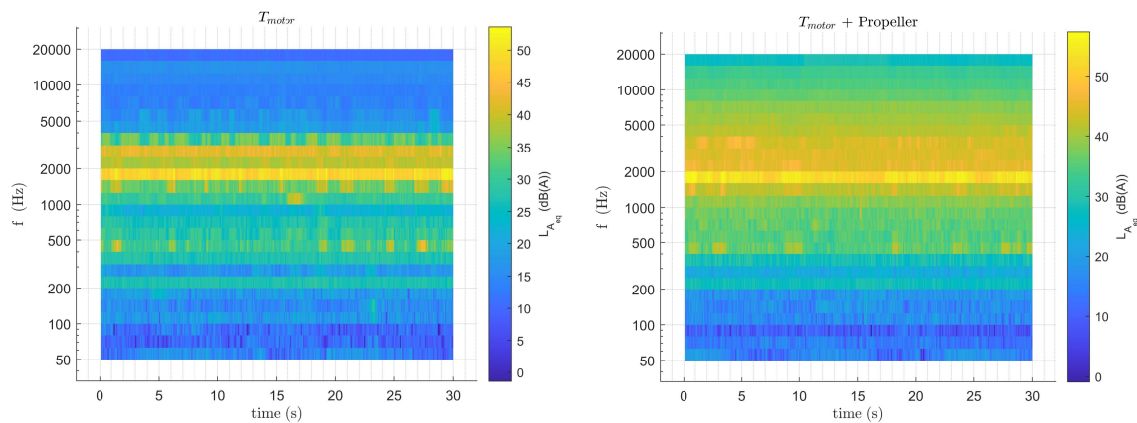

Figure 14. $L_{A_{eq}}$ spectrogram at 1860 rpm - Tmotor(left), Tmotor + propeller (right).

The test has shown that the T-motor + propeller configuration is prevalent, in terms of $L_{A_{eq}}$ over the T-motor configuration. In Figure 16 it is possible to notice that in correspondence of an angular velocity of 1140 and 1500 rpm, this trend is not fulfilled and the T-motor configuration shows a higher noise level due to distinct tones appearing in the 3rd octave band of center 1000, 1250 and 1600 Hz. In correspondence with an angular velocity of 2820 rpm, an 8 dB(A) difference of the $L_{A_{eq}}$ can be highlighted. The same difference becomes 6 dB(A) in the case of the afore-mentioned 1140 and 1500 rpm conditions which can be stated as critical in terms of motor functioning.
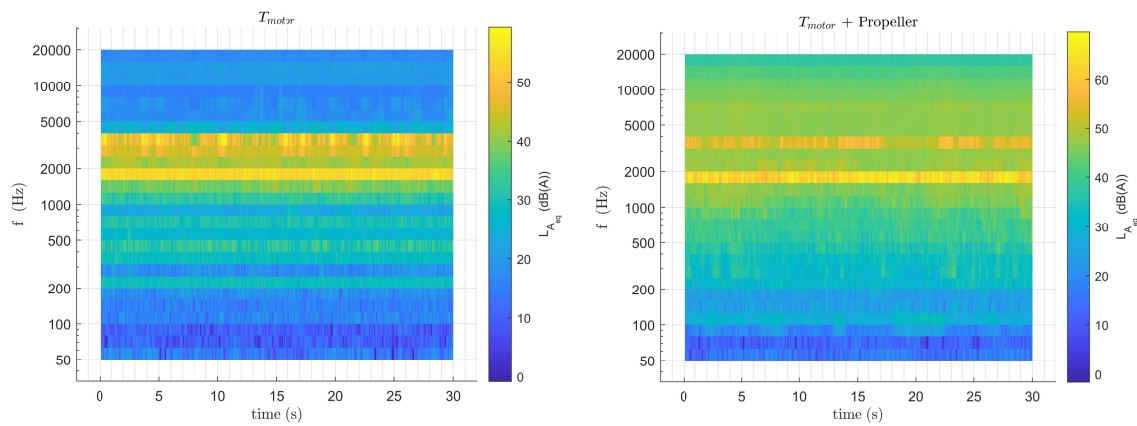
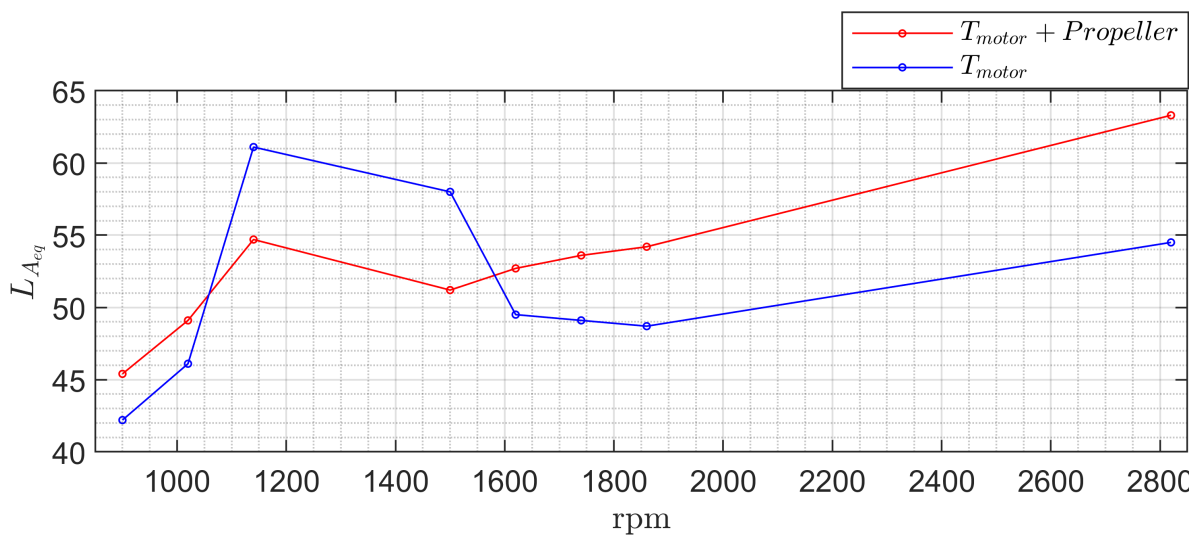**Figure 15.** $L_{A_{eq}}$ spectrogram at 2820 rpm - Tmotor(left), Tmotor + propeller (right).

Figure 16. $L_{A_{eq}}$ varying rpm. Isolated propeller noise characterization.

3.2. Counter rotating propellers performances evaluation

A sensitivity analysis has been carried by considering different relative positions between the two propellers and measuring the thrust and the noise in correspondence of multiple angular velocity values. Three values of distances between the propellers h have been considered:
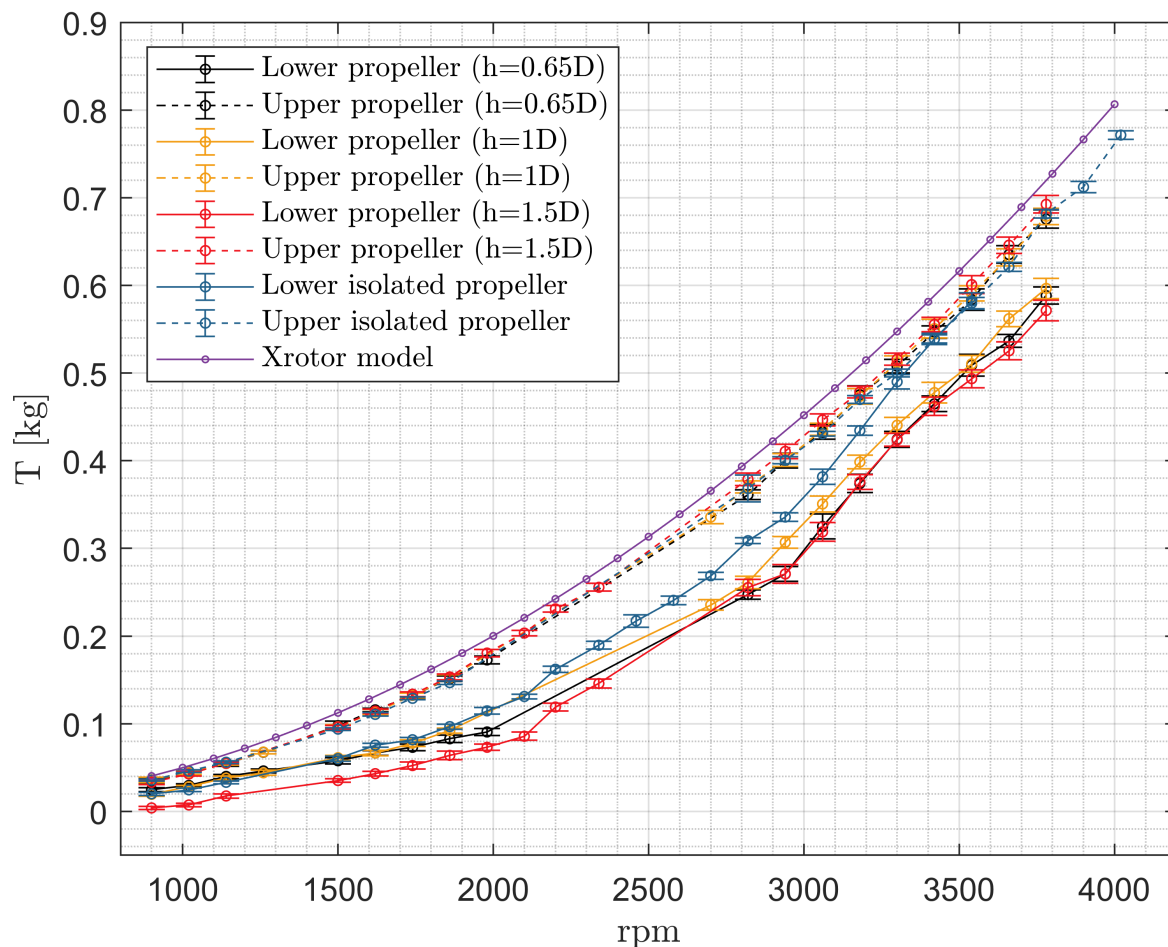
- condition A: $h = 1.5D$;
- condition B: $h = 1D$;
- condition C: $h = 0.65D$.

3.2.1. Thrust comparative analysis

The comparative thrust analysis brings some interesting considerations concerning both the upper and the lower propeller and their behaviour for decreasing distance. The standard deviation associated with the data set at the specific angular velocity has been reported to be not sensitive to the distance between the two propellers. It is possible to notice that the standard deviation is always contained into the 5% of the rated output range defined by the cell manufacturer. This eventuality shows an overall good behavior of the load cell acquisition system which is not affected by the changing of the position of the electric components. The thrust performance of the upper propeller is not highly affected by the distance parameter. This might be justified by the fact that, due to the test configuration, it still operates upstream but it is not heavily influenced by inducted velocity generated by the lower propeller.

Looking at Figure 17 it is possible to highlight that upper propellers characteristic curves show a good agreement to the numerical model which is reported to be slightly oversizing concerning the isolated upper propeller (0.010 kg at 3780 rpm).

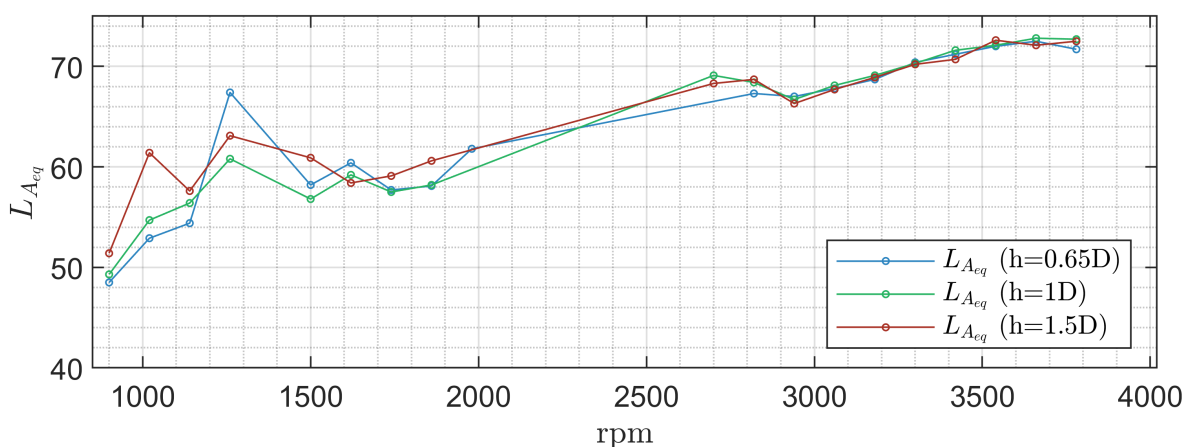**Figure 17.** Thrust varying rpm for test condition A, B, C and isolated propellers.

The lower propeller shows some interesting results: the performance of the isolated lower propeller is always prevalent to the ones in correspondence of the three test conditions A, B, C. The thrust performance of the lower propeller resents negatively from this aspect since the lower rotor is operating in part in the slipstream of the upper rotor. The upper rotor is experiencing an additional induced flow velocity due to its location in the induced inflow velocity field of the lower rotor while the lower rotor works, instead, in the contracted wake of the upper propeller [37]. As a result, the overall thrust produced by the pressure difference is reduced (Figure 18). From the viewpoint of the pressure interaction, therefore, two propellers should be located as far as possible [38].
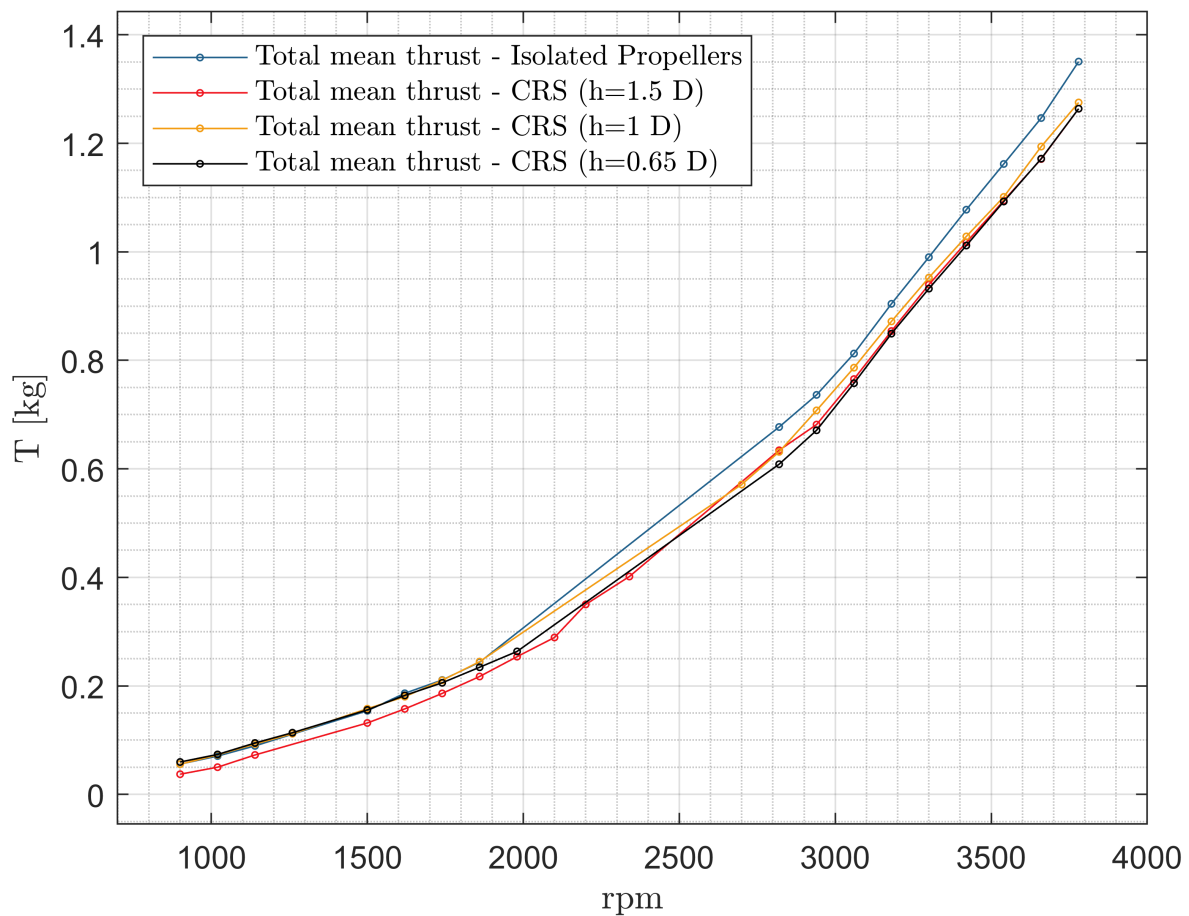
Figure 18. Total mean thrust varying rpm for test condition A, B, C and isolated propellers.

3.2.2. Noise comparative analysis

By means of a comparative analysis of the noise results (Figure 19) it is possible to notice two separated regions: for angular velocities lower than 1500 rpm, the noise level is predominantly associated with a motor contribution while, in the other cases, the T-motor + propeller configuration is predominant. In the T-motor + propeller prevalence region, the $L_{A_{eq}}$ grows with the angular velocity.

Figure 19. $L_{A_{eq}}$ varying rpm for test condition A, B and C.

In the lower rpm region occurs a higher variability of the $L_{A_{eq}}$ not attributable to the distance between the propellers but to some motor or rig-related occurrences in correspondence of 1260 rpm.

This consideration is triggered by the T-motor prevalence in that angular velocity range. From a structural point of view, for an angular velocity of 1260 rpm, a minor structure resonance occurs so that the measured noise is generated from the mechanical components and not from the motor itself. For angular velocities higher than 2820 rpm, the $L_{A_{eq}}$ is almost constant with respect to the distance between the propellers. This aspect can be highlighted considering the frequency spectra of the test condition "C" (Figures 20-24).
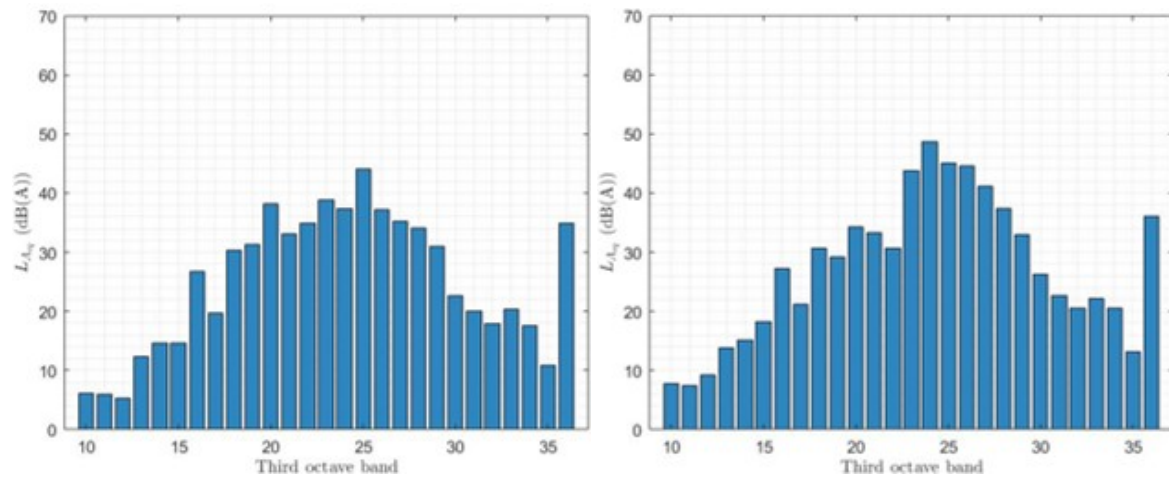

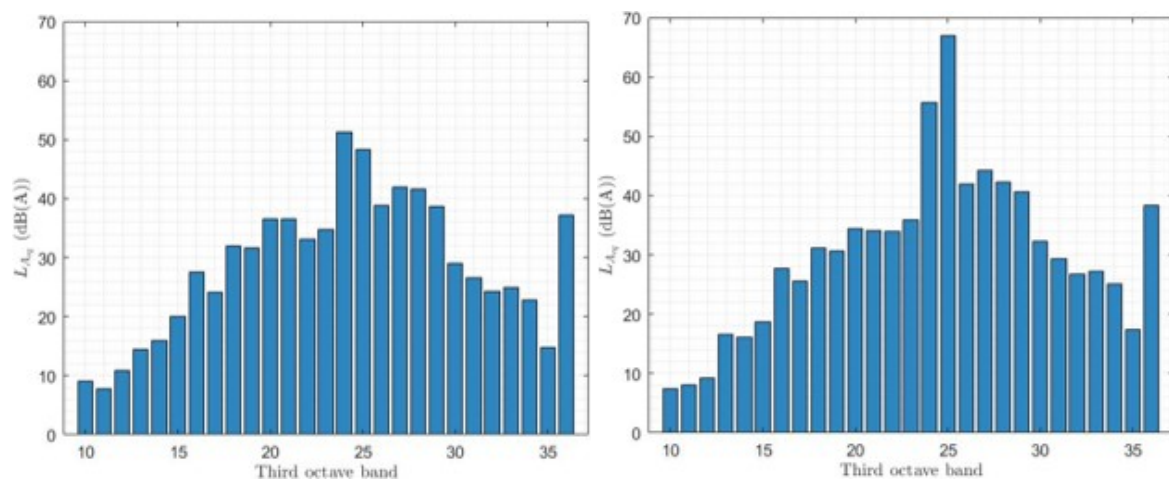**Figure 20.** $L_{A_{eq}}$ in 3rd octave band in the condition C, 900 rpm (left) and 1020 rpm (right).

Figure 21. $L_{A_{eq}}$ in 3rd octave band in the condition C, 1140 rpm (left) and 1260 rpm (right).
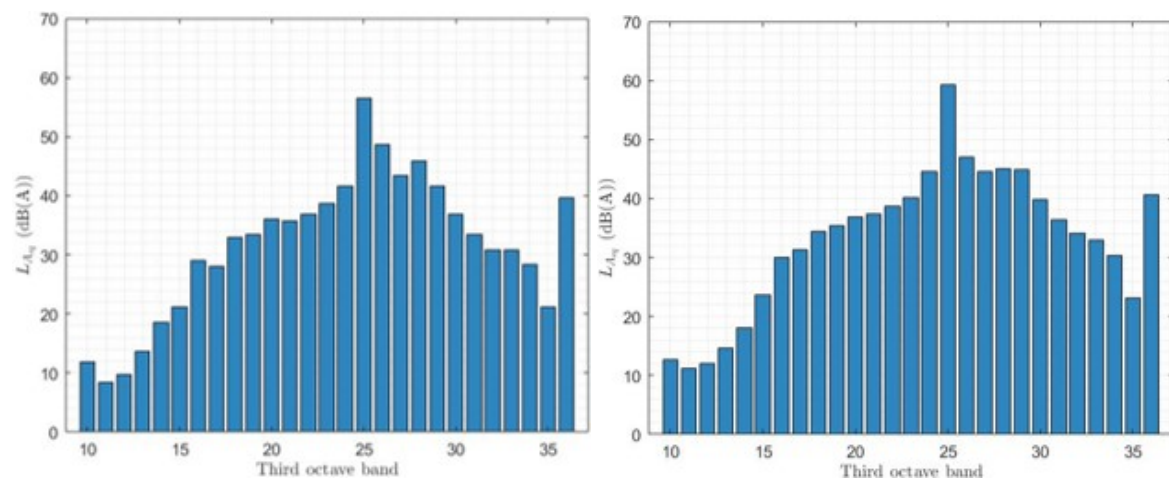

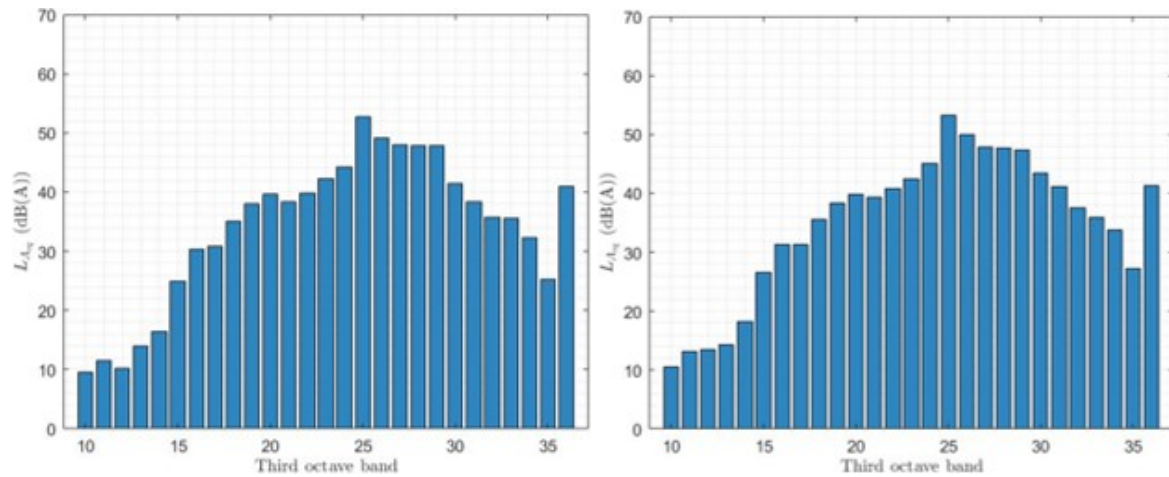**Figure 22.** $L_{A_{eq}}$ in 3rd octave band in the condition C, 1500 rpm (left) and 1620 rpm (right).

Figure 23. $L_{A_{eq}}$ in 3rd octave band in the condition C, 1740 rpm (left) and 1860 rpm (right).
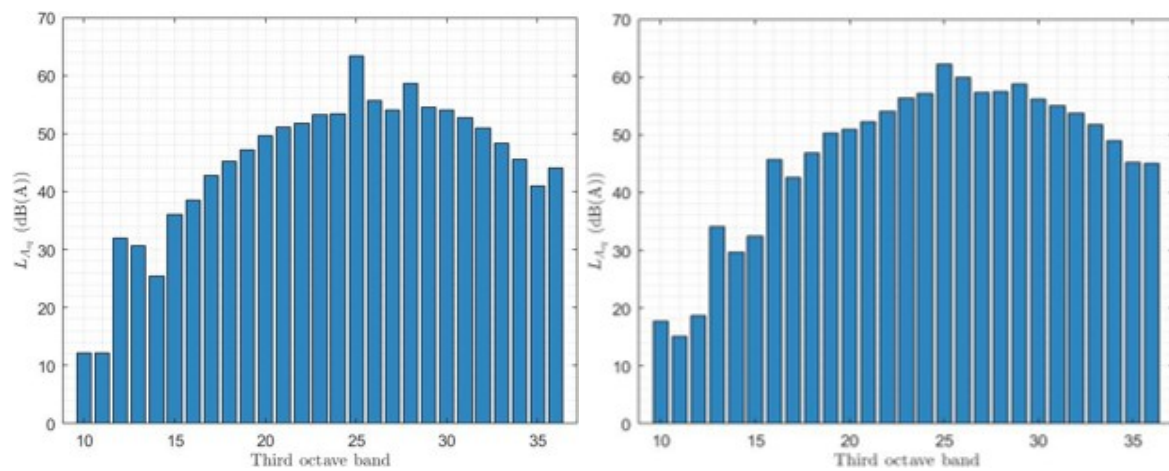

Figure 24. $L_{A_{eq}}$ in 3rd octave band in the condition C, 2700 rpm (left) and 3180 rpm (right).

4. Conclusions and remarks

This work was aimed to the design, manufacturing and testing a new test facility for coaxial counter-rotating propellers for multirotors application. This facility has lately been used to prove that the distance between the two propellers is a sensitive parameter concerning both the thrust and the acoustic performances. Noise characterization of both the T-motor and the T-motor + propeller configuration has been carried out: in correspondence of an angular velocity of 1140 and 1500 rpm, the T-motor configuration shows a higher noise level due to distinct tones appearing in the third octave band of centerbands 1000, 1250 and 1600 Hz; for the other tested velocities, the T-motor + propeller has been prevalent. From a thrust point of view, the isolated propellers analysis has shown inferior performances of the lower line concerning the angular velocity range between [900-3480] rpm. Further analysis on the complete counter-rotating system has shown that the trust produced by the single propellers, for different values of the inter-axis distance, is lower than the trust produced by the same propellers when run in isolated conditions. The total mean thrust has shown no relevant variation for the three mentioned distance conditions (1.5 D, 1 D, and 0.65 D). The $L_{A_{eq}}$ has shown higher variability at lower rpm regimes while, at angular velocities higher than 2820 rpm, it is identical concerning the three distance conditions. Finally, as the angular velocity increases, the noise becomes more distributed in frequency.

Future development of this work will regard the employment of an ammeter to observe the reduction of the torque motors exert when the two propellers work together. As a consequence, an improvement of the efficiency should be observed.

References

1. National Academies of Sciences, Engineering and Medicine, *Advancing Aerial Mobility: A National Blueprint*, Washington DC, **2020**. DOI: 10.17226/25646.

2. Sheehan, V. *Vertical Flight Society Electric VTOL Directory Hits 600 Concepts*, The Vertical Flight Society, Fairfax, Virginia, USA, **2022**.

3. Rashad, R.; Goerres, J.; Aarts, R.; Engelen, J. BC and Stramigioli, S. *Fully actuated multirotor UAVs: A literature review*, IEEE Robotics & Automation Magazine, IEEE, **2020**. DOI: 10.1109/MRA.2019.2955964.

4. Coluccia, A.; Parisi, G. and Fascista, A. *Detection and classification of multirotor drones in radar sensor networks: A review*, Sensors, Multidisciplinary Digital Publishing Institute, **2020**. DOI: 10.3390/s20154172.

5. Withrow-Maser, S.; Malpica, C. and Nagami, K. *Multirotor Configuration Trades Informed by Handling Qualities for Urban Air Mobility Application*, NASA Ames Research Center, **2020**.

6. Mahony, R.; Kumar, V. and Corke, P. *Multirotor aerial vehicles: Modeling, estimation, and control of quadrotor*, IEEE Robotics and Automation magazine, Institute of Electrical and Electronics Engineers Inc., **2012**. DOI: 10.1109/MRA.2012.2206474.

7. Prior, S.D. *Reviewing and Investigating the Use of Co-Axial Rotor Systems in Small UAVs*, Autonomous Systems Laboratory, Department of Product Design and Engineering, School of Engineering and Information Sciences, Middlesex University, Trent Park Campus, London, UK, **2010**. DOI: 10.1260/1756-8293.2.1.1.

8. Cédric, M. S. *Optimizing a Coaxial Propulsion System to a Quadcopter*. Dept. Engenharia Mecânica, Instituto Superior Técnico, Av. Rovisco Pais, 1049-001 Lisboa, Portugal.

9. McCormick, B. W. *Aerodynamics of V/STOL flight*; Academic Press, INC.; Publishing House: New York, USA, 1967; p. 337.

10. Stepniewski, W. Z. and Keys, C. N., *Blade Element Theory*, In *Rotary-Wing Aerodynamics*, Dover Publications, Inc., **1984**.

11. Wald, Q. R. *The aerodynamics of propellers*, Progress in Aerospace Sciences, Elsevier, **2006**. DOI: 10.1016/j.paerosci.2006.04.001.

12. Theodorsen, T. *Theory of Propellers*, McGraw-Hill, **1948**.

13. Emmanuel Branlard, *Wind Turbine Aerodynamics and Vorticity-Based Methods*, Research Topics in Wind Energy, vol 7. Springer.

14. Leishman, J.G. *Principles of Helicopter Aerodynamics*, Cambridge University Press, 2nd Ed. **2006**. ISBN: 978-0-521-85860-1.

15. Manetti, E. *CFD Analysis, Experimental Validation and Optimization of an Octocopter Drone with Counter-Rotating Propellers*, Aerotec. Missili Spaz. 102, 17–27 **2023**. DOI:https://doi.org/10.1007/s42496-022-00140-7

16. Manetti, E. *An Experimental and Numerical Study of the Aerodynamic Interaction Between Tandem Overlapping Propellers*, Aerotec. Missili Spaz. 102, 77–89 **2023**. DOI:https://doi.org/10.1007/s42496-022-00138-1

17. Kotwicz Herniczek, M. T., Feszty, D., Meslioui, S. A., Park, J., and Nitzsche, F. *Evaluation of acoustic frequency methods for the prediction of propeller noise*, AIAA Journal, 57(6) **2019**. DOI:https://doi.org/10.2514/1.J056658

18. Hambrey, J., Kotwicz Herniczek, M. T., Feszty, D., Meslioui, S. A., and Park, J. *Comparison of three popular methods for the prediction of high speed propeller noise*, 23rd aiaa/ceas aeroacoustics conference **2017**. DOI:https://doi.org/10.2514/6.2017-3917

19. Hambrey, J., Feszty, D., Meslioui, S. A., and Park, J. *Acoustic Prediction of High Speed Propeller Noise Using URANS and a Ffowcs Williams-Hawkings Solver*, In 35th AIAA Applied Aerodynamics Conference **2017**.

20. Xue, D., Yan, Q., Li, Z., and Wei, K. *Multidisciplinary Optimization Design of Low-Noise PropellersMultidisciplinary Optimization Design of Low-Noise Propellers*, Aerospace 10(3) **2023**. DOI:https://doi.org/10.3390/aerospace10030254

21. Holmes, J.B.; Durham, M.H. and Tarry, S.E. *Small aircraft transportation system concept and technologies.*, J Aircraft **2004**;41:26–35. DOI: 10.2514/1.3257.

22. Ffowcs Williams, J. E.; Hall, L.H. *Aerodynamic sound generation by turbulent flow in the vicinity of a scattering half plane*, Journal of Fluid Mechanics, **1970**. DOI: 10.1017/S0022112070000368.

23. Sinibaldi, G. and Marino, L. *Experimental analysis on the noise of propellers for small UAV*, Department of Mechanical and Aerospace Engineering, University of Rome La Sapienza, Roma, Italy. **2013** DOI: 10.1016/j.apacoust.2012.06.011.

24. Suzuki, Y. and Takeshima, H. *Equal-loudness-level contours for pure tones*. The Journal of the Acoustical Society of America, **2004**. DOI: 10.1121/1.1763601

25. T-motor, *T-motor Antigravity 4004 KV300 – 2PCS/SET*. Available online: https://robocraft.co.in/product/t-motor-antigravity-4004-kv300-2pcs-set

26. Picotronik, *Serie ABB(70)*, Available online: https://www.picotronik.it/wp-content/uploads/2016/08/ABB_7000.pdf

27. AVIA-Semiconductor, *24-Bit Analog-to-Digital Converter*, Available online: https://cdn.sparkfun.com/datasheets/Sensors/ForceFlex/hx711_english.pdf

28. Bramwell, A.R.S. *Helicopter Dynamics*, Edward Arnold.**1976**.

29. Gessow, A. and Myers, G.C. *Aerodynamics of the Helicopter*, The Macmillan Company. **1952**.

30. Johnson, W. *Helicopter Theory*, Princeton University Press, Dover Publications **1984**.

31. Leishman, J. G., *Principles of Helicopter Aerodynamics*, Cambridge Aerospace Series. **2000**.

32. Capone, A., Di Felice, F., and Pereira, F. A *On the flow field induced by two counter-rotating propellers at varying load conditions*, Ocean Engineering, 221 **2021**. DOI:https://doi.org/10.1016/j.oceaneng.2020.108322

33. Lugt, H.J. *Autorotation*. Annual Review of Fluid Mechanics, 15(1),**1983**; 123-147. DOI: 10.1146/annurev.fl.15.010183.001011.

34. Houston, S.S. and Brown, R.E. *Rotor-wake modeling for simulation of helicopter flight mechanics in autorotation*. Journal of aircraft, 40(5), 938-945. **2003**. DOI: 10.2514/2.6870.

35. Houston, S.S. *Modeling and analysis of helicopter flight mechanics in autorotation*. Journal of aircraft, 40(4), 675-682. **2003**. DOI: 10.2514/2.3171.

36. NTi Audio, *https://www.nti-audio.com/Portals/0/data/en/XL2-Specifications.pdf*

37. Thiele, M. Obster, M. and Hornung, M. *Aerodynamic Modeling of Coaxial Counter-Rotating UAV Propellers*. 8th Biennial Autonomous VTOL Technical Meeting, Mesa, AZ, **2019**.

38. Keh-Sik Min; Bong-Jun Chang and Heung-Won Seo *Study on the Contra-Rotating Propeller system design and full-scale performance prediction method*, Hyundai Heavy Industries, Co. Ltd., Ulsan, Korea. **2009** DOI: 10.2478/IJNAOE-2013-0004.